



Quantum gate sets for lattice QCD in the strong-coupling limit: $N_f = 1$

Michael Fromm^{1*}, Owe Philipsen¹, Wolfgang Unger² and Christopher Winterowd¹

*Correspondence:

mfromm@itp.uni-frankfurt.de

¹Institut für Theoretische Physik,
Goethe-Universität, Frankfurt am
Main, Germany

Full list of author information is
available at the end of the article

Abstract

We derive the primitive quantum gate sets to simulate lattice quantum chromodynamics (LQCD) in the strong-coupling limit with one flavor of massless staggered quarks. This theory is of interest for studies at non-zero density as the sign problem can be overcome using Monte Carlo methods. In this work, we use it as a testing ground for quantum simulations. The key point is that no truncation of the bosonic Hilbert space is necessary as the theory is formulated in terms of color-singlet degrees of freedom (“baryons” and “mesons”). The baryons become static in the limit of continuous time and decouple, whereas the dynamics of the mesonic theory involves two qubits per lattice site. Lending dynamics also to the “baryons” simply requires to use the derived gate set in its controlled version.

Keywords: Hamiltonian lattice gauge theory; Quantum computing

1 Introduction

Recently, there has been considerable interest generated by proposals for quantum simulations of gauge theories in high-energy physics. This interest has spread to lattice gauge theory (LGT), and in particular, to lattice quantum chromodynamics (LQCD). This development promises to allow direct access to real-time physics as well as to the physics of dense nuclear matter from LQCD. Considerable progress has been made in the universal gate-based approach both in the methods needed [1–4] as well as their applications to theories with both discrete and continuous gauge groups to varying levels of approximation.¹

Although from current estimates it seems that near-term, large-scale simulations of LQCD on quantum computers are infeasible [6], one can still define physically interesting problems which can be studied in the noisy intermediate-scale quantum (NISQ) era [7]. In the gate-based approach, one is of course forced to work in the Hamiltonian formulation. In the case of LGT, the Hamiltonian formulation appeared quite early [8] but was of secondary interest due to the success of Markov chain Monte Carlo methods which

¹See [5] for a recent experimental proposal to realize non-Abelian LGTs using analog quantum simulations.

rely on the Lagrangian formulation. Another pioneering study identified the mapping of operators appearing in the Hamiltonian into spin operators for continuous gauge groups assuming a cutoff in the infinite-dimensional Hilbert space of the gauge bosons [9]. This line of analysis has also been extended to fermions [10]. In order to alleviate the systematic effects of Hilbert space truncation, one can attempt to improve the Kogut-Susskind Hamiltonian by adding terms which reproduce the desired physics for a given cutoff. This has very recently been done for the strong-coupling limit using a similarity renormalization group approach [11].

The strong-coupling limit of lattice QCD has been a long-standing field of interest, both in the Wilson and staggered formulations. Of particular interest are the reformulation of the theory in color-singlet degrees of freedom and their first numerical simulations [12, 13]. This work was mainly motivated by the possibility to either cure or alleviate the sign problem, and hence study LGT systems at non-zero baryon density. Equipped with new algorithms, these studies were revisited some years later, leading to a complete mapping of the phase diagram for one staggered flavor in the strong coupling limit ($\beta = 0$) [14] and beyond [15]. All of the above-mentioned studies start from the Lagrangian formulation and thus, in principle, have little to say about real-time evolution of quantum states. Recently, a continuous-time partition function has been formulated leading to the construction of a Hamiltonian describing the physics of the strong-coupling limit with $N_f = 1$ flavors of massless staggered fermions [16]. Further efforts were undertaken to extend this to the case of $N_f = 2$ [17, 18].

There exists then ample motivation to study the strong-coupling limit of lattice QCD from the perspective of quantum simulations: For one, as the gauge degrees of freedom can be integrated out exactly in any spatial dimension, Gauss' law is fulfilled implicitly. Secondly, the resulting variables form a discrete set of physical, color-singlet degrees of freedom (mesons and baryons) governed by a local, sparse nearest-neighbor Hamiltonian. Finally, due to the mildness of the sign problem in the Euclidean formulation, cross checks between the formulations can be performed in the extended parameter space of finite μ , T at *continuous* Euclidean time. We restrict ourselves to the case of massless quarks which is conceptually simpler [19] and exhibits an exact remnant chiral symmetry. It therefore seems natural to map the strong-coupling Hamiltonian onto the degrees of freedom relevant for quantum simulations, starting with the one-flavor, $\beta = 2N_c/g^2 = 0$ case which is the subject of our current study.

2 Background

The Hamiltonian we study is derived from the continuous Euclidean time limit of strong-coupling lattice QCD with staggered fermions. Strong-coupling lattice QCD can be formulated in terms of dual variables in order to tackle the sign problem, with the full $\mu_B - T$ phase diagram accessible through Monte Carlo simulations. The partition function of the discrete system for one flavor of massless staggered fermions is given by

$$Z(\gamma, a_\tau, N_\tau) = \int \mathcal{D}\chi \mathcal{D}\bar{\chi} \mathcal{D}U e^{\mathcal{S}_F}, \quad (1)$$

where

$$S_F = \sum_x \left[\gamma \eta_0(x) (\bar{\chi}(x) e^{a_\tau \mu_q} U_0(x) \chi(x + \hat{0}) - \bar{\chi}(x + \hat{0}) e^{-a_\tau \mu_q} U_0^\dagger(x) \chi(x)) + \sum_{i=1}^d \eta_i(x) (\bar{\chi}(x) U_i(x) \chi(x + \hat{i}) - \bar{\chi}(x + \hat{i}) U_i^\dagger(x) \chi(x)) \right] \tag{2}$$

is the staggered quark action S_F on an anisotropic lattice of extent $N_\tau \times L^d$. As the temperature is given by $T = (a(\beta)N_\tau)^{-1}$ on an isotropic lattice, it requires anisotropic lattices to continuously vary the temperature at fixed inverse gauge coupling. At strong coupling $\beta = 0$, the lattice spacing a is maximally coarse, while the temporal lattice spacing a_τ will be sent to zero. The non-perturbative relation between the bare anisotropy γ , introduced above as a prefactor to favor temporal over spatial fermion hops, and the physical anisotropy $\xi \equiv \frac{a}{a_\tau}$, has been determined non-perturbatively for various N_τ and towards the continuous time limit $N_\tau \rightarrow \infty$ [20]. The resulting temperature in lattice units is $aT = \frac{\xi(\gamma)}{N_\tau}$, which simplifies in the continuous time limit to $aT = \kappa \frac{\gamma^2}{N_\tau}$ with $\kappa = 0.7971(3)$. This is close to the mean-field result where $\kappa = 1$.

Owing to the limit of infinite gauge coupling, the gauge link integration $\int DU$ in Eq. (1) can be done exactly [13], followed by the Grassmann integration. This results in the partition function of a dimer model [16, 21]

$$\mathcal{Z}(\gamma, a_\tau \mu_B, N_\tau) = \mathcal{N}(\gamma) \sum_{\{k, \ell\}} \prod_{x \in \Lambda_M} \left(\delta_{\sum_\mu k_\mu(x), 3} \frac{(3 - k_0(x))!}{k_0(x)!} \prod_{i=1}^d \frac{(3 - k_i(x))!}{k_i(x)!} \gamma^{-2k_i(x)} \right) \times \prod_{\ell \subset \Lambda_B} \left(\sigma(\ell) \prod_{(x, \mu) \in \ell} \exp((\delta_{\hat{\mu}, +\hat{0}}(\ell) - \delta_{\hat{\mu}, -\hat{0}}(\ell)) a_\tau \mu_B) \prod_{i=1}^d (\gamma^{-3\delta_{\mu i}}) \right), \tag{3}$$

with the $(3 + 1)$ -dim. lattice volume Λ decomposed into the disjoint union of mesonic sites Λ_M and baryonic sites Λ_B . The integers $k_\mu \in \{0, \dots, 3\}$ are dimers, the selfavoiding loops ℓ denote baryons worldlines. Note that the sign $\sigma(\ell) \in \{+1, -1\}$ can be negative for nontrivial baryon loops, but $\sigma(\ell) = 1$ for static baryons. The normalization $\mathcal{N}(\gamma)$ can be disregarded. The number of spatial meson hops depends on the temperature, but remains finite at fixed aT as $N_\tau \rightarrow \infty$. This results in the suppression of spatial meson hops of orders higher than γ^{-2} in units of a_t , simplifying Eq. (3) significantly:

$$\mathcal{Z}(\gamma, a_\tau \mu_B, N_\tau) = \sum_{\{\Sigma_M, \Sigma_B\}} \left(\sum_{\substack{k_0 \in \{0, \dots, 3\} \\ k_i \in \{0, 1\}}}^{\text{GC}} \prod_{\substack{(\vec{x}, \tau) \in \Lambda_M \\ \{x | k_i(x) = 1\}}} \frac{\nu(k_0^- | k_0^+)_{(\vec{x}, \tau)} \nu(k_0^- | k_0^+)_{(\vec{x} + \hat{i}, \tau)}}{\gamma^2} \right) (2 \cosh(\mu_B/T))^{|\Sigma_B|}, \tag{4}$$

with Σ_M and Σ_B denoting the spatial mesonic and baryonic sublattices respectively, which no longer depend on $\tau \in \{0, \dots, N_\tau - 1\}$. The mesonic contribution has non-trivial weights whenever, at some time index τ , a meson hop between nearest neighbors $\langle \vec{x}, \vec{x} + \hat{i} \rangle$ occurs. Here $\nu_{(\vec{x}, \tau)}$ depends on the temporal dimers k_0^\pm just before/after the spatial dimer location, and due to $k_0^- + k_0^+ + 1 = 3$, the only possible transitions are $\nu_L \equiv \nu(0|2) = \nu(2|0) = 1$,

$v_T \equiv v(1|1) = 2/\sqrt{3}$. In between spatial meson exchange, the temporal dimers at a given site \vec{x} form states that can be identified as meson occupations, $m = \{0, \pi, 2\pi, 3\pi\}$, which correspond to a conserved pion current. For the baryonic contribution, spatial hops are suppressed and we have used $\mu_B/T = a_\tau \mu_B N_\tau$ for the baryon chemical potential $\mu_B = 3\mu_q$.

One finally takes the limit $N_\tau \rightarrow \infty$ of Eq. (4), by substituting γ^2 with aTN_τ , such that the pion exchange between nearest neighbors can be written as an exponential, and the vertices can be expressed with matrices \hat{J}^\pm which raise or lower the meson occupation number, resulting in the following partition function:

$$\mathcal{Z}_{\text{CT}}(aT, a\mu_B) = \text{Tr}_{\mathbb{H}_h} [e^{(-\hat{H} + \hat{N} a\mu_B)/aT}] \tag{5}$$

with the Hamilton and number operators

$$\hat{H} = -\frac{1}{2} \sum_{\langle \vec{x}, \vec{y} \rangle} (\hat{J}_x^+ \hat{J}_y^- + \hat{J}_x^- \hat{J}_y^+), \quad \hat{N} = \sum_{\vec{x}} \hat{\omega}_x. \tag{6}$$

The corresponding ladder operators $\hat{J}_x^- = (\hat{J}_x^+)^T$ are:

$$\hat{J}_x^+ = \left(\begin{array}{cccc|cc} 0 & 0 & 0 & 0 & & \\ v_L & 0 & 0 & 0 & & \\ 0 & v_T & 0 & 0 & & \\ 0 & 0 & v_L & 0 & & \\ \hline & & & & 0 & 0 \\ & & & & 0 & 0 \end{array} \right), \quad \hat{\omega} = \left(\begin{array}{cccc|cc} 0 & 0 & 0 & 0 & & \\ 0 & 0 & 0 & 0 & & \\ 0 & 0 & 0 & 0 & & \\ 0 & 0 & 0 & 0 & & \\ \hline & & & & 1 & 0 \\ & & & & 0 & -1 \end{array} \right). \tag{7}$$

The trace in Eq. (5) is over the Hilbert space $\mathbb{H}_h = \bigotimes_{\vec{x} \in \Sigma} \mathbb{H}_{h_{\vec{x}}}$, where the local Hilbert space $\mathbb{H}_{h_{\vec{x}}}$ is 6 dimensional, with states $|h\rangle = |m, b\rangle \in \mathbb{H}_{h_{\vec{x}}}$ and a basis $|h_i\rangle$ of 6 hadronic states per spatial lattice site,

$$|h_i\rangle \in \{0, \pi, 2\pi, 3\pi, B^+, B^-\}. \tag{8}$$

The nature and dimensionality of these states can be explained by the fact that the gauge integration in Eq. (1), carried out analytically in the limit of infinite gauge coupling ($\beta = 0$), results in the reformulation of the theory of Eq. (2) in terms of color-singlet degrees of freedom, “baryons” and “mesons”. The subsequent Grassmann integration and continuous time limit constrains the site occupation to $0, \dots, N_c$ “pions”, $N_c = 3$, alternatively a site may be occupied by a “baryon” or “anti-baryon”.² By redefining the meson occupation numbers as $|s\rangle = |m - 3/2\rangle$, a particle-hole symmetry becomes evident, as the mesonic creation and annihilation operators fulfill the following algebra:

$$[\hat{J}^+, \hat{J}^-] = \begin{pmatrix} -1 & 0 & 0 & 0 \\ 0 & -1/3 & 0 & 0 \\ 0 & 0 & 1/3 & 0 \\ 0 & 0 & 0 & 1 \end{pmatrix},$$

²This should be contrasted to the local, infinite dimensional bosonic Hilbert space of pure LGT, when starting from the Kogut-Susskind Hamiltonian e.g. in the representation basis [2] or group basis [1].

$$\begin{aligned}\hat{J}_1 &= \frac{\sqrt{3}}{2}(\hat{J}^+ + \hat{J}^-), & \hat{J}_2 &= \frac{\sqrt{3}}{2i}(\hat{J}^+ - \hat{J}^-), \\ \hat{J}_3 &= i[\hat{J}_1, \hat{J}_2] = \frac{3}{2}[\hat{J}^+, \hat{J}^-], & \hat{J}^2 &= \frac{15}{4}\mathbb{1}.\end{aligned}\quad (9)$$

This corresponds to a 4-dim. representation of $SU(2)$ with $|j, m\rangle \equiv |3/2, s\rangle$. This construction can be extended to a $N_f = 2$ Hamiltonian [17, 18], resulting in:

$$Z_{CT}(aT, a\mu_B, a\mu_I) = \text{Tr}_{\mathbb{H}_0} [e^{(-\hat{\mathcal{H}} + \hat{\mathcal{N}}_B a\mu_B + \hat{\mathcal{N}}_I a\mu_I)/aT}], \quad (10)$$

where the Hamiltonian is now composed of a sum of 4 contributions, one for each pion $\pi \in \{\pi^+, \pi^-, \pi_u, \pi_d\}$:

$$\hat{\mathcal{H}} = -\frac{1}{2} \sum_{(\vec{x}, \vec{y})} \sum_{Q_i \in \{\pi^+, \pi^-, \pi_u, \pi_d\}} (\hat{J}_{Q_i, \vec{x}}^+ \hat{J}_{Q_i, \vec{y}}^- + \hat{J}_{Q_i, \vec{x}}^- \hat{J}_{Q_i, \vec{y}}^+). \quad (11)$$

In addition to the baryon number operator $\hat{\mathcal{N}}_B$, the $N_f = 2$ partition function also contains an isospin number operator $\hat{\mathcal{N}}_I$. The number of distinct hadronic states $|h\rangle$ is now 92, of which 50 states are purely mesonic. It turns out that all the matrix elements in $\hat{J}_{Q_i}^\pm$ are positive, allowing one to study both non-zero baryon and isospin chemical potential.

Another possible extension of the Hamiltonian Eq. (6) is to perform the strong-coupling expansion [22] before taking the continuous time limit, which results in only temporal plaquettes contributing. Both the $N_f = 2$ formulation and the inclusion of the leading-order gauge corrections to the Hamiltonian will be discussed in a forthcoming publication.

3 Implementation and results

The Hamiltonian $\hat{\mathcal{H}}$ and the number operator $\hat{\mathcal{N}}$, as defined in Eq. (6), have a block-diagonal structure, with the states $|h\rangle_x$ of the local Hilbert space being a direct *sum* of mesonic and baryonic occupational states, $|h\rangle_x = |m\rangle_x \oplus |b\rangle_x$. As a practical consequence, this allows us to qubitize the Hamiltonian Eq. (6) in the mesonic sector and baryonic sector independently. We begin with the former.

3.1 Mesonic gate sets

The four-dimensional local meson states $|m_i\rangle \in \{0, \pi, 2\pi, 3\pi\}$ can be encoded with two qubits. The Hamiltonian $\hat{\mathcal{H}}$ represents a nearest-neighbor meson hopping term, seen through the action of the raising and lowering operators, \hat{J}^+ and \hat{J}^- , respectively, on the local Hilbert space. Such a local, low-dimensional Hamiltonian can be qubitized with standard methods [23] as we summarize below for the case of 1 + 1-dim. The method, of course, is completely general and can be applied to higher dimensions.

We start by partitioning the lattice Hamiltonian into mutually commuting even and odd parts

$$\hat{\mathcal{H}} = \sum_{x_e} \hat{\mathcal{H}}_{x_e} + \sum_{x_o} \hat{\mathcal{H}}_{x_o}, \quad (12)$$

where $\hat{\mathcal{H}}_{x_{e/o}}$ both have the nearest-neighbor nn -form of Eq. (6), and the labels “even” and “odd” refer to the bonds of the one-dimensional lattice. Using the Pauli decomposition

$\mathcal{H}_{x_{e/o}} = \sum_i c_i P_i$ into Pauli strings $P_i \in \{I, X, Y, Z\}^{\otimes 4}$, the remaining tasks are that of partitioning the P_i into sets (“families”) of mutually commuting terms, which can then be simultaneously diagonalized. The Pauli decomposition yields eighteen four-qubit terms (two qubits for the neighboring sites x and y , respectively) which can easily be grouped into four families.³ The partition of the operators into four families Fam_k takes the form

$$\begin{aligned}\text{Fam}_1 &= \{(IX)_x(YY)_y, (IY)_x(YX)_y, x \leftrightarrow y \text{ terms}\}, \\ \text{Fam}_2 &= \{XXYY, XYYX, YYXX, YXXY\}, \\ \text{Fam}_3 &= \{IXXX, IYXY, XXIX, XYIY\}, \\ \text{Fam}_4 &= \{YYYY, YXYX, IXIX, IYIY, XXXX, XYXY\},\end{aligned}\tag{13}$$

where the big endian convention is used. The individual terms are multiplied by the coefficients $c_j^{(k)}$ which are listed in the [Appendix](#) (Eq. (17)). Each of the Fam_k can be diagonalized simultaneously using the tableau formalism described in [25], yielding the sets

$$\begin{aligned}\text{Diag}_{\text{Fam}_{1/2}} &= \{IIZZ, IZZZ, ZIIZ, ZZIZ\}, \\ \text{Diag}_{\text{Fam}_3} &= \{IZZI, IZZZ, ZZII, ZZIZ\}, \\ \text{Diag}_{\text{Fam}_4} &= \{ZZZZ, ZIZZ, IIZZ, IZIZ, IIZZ, IZZZ\}.\end{aligned}\tag{14}$$

The transformations V_k which diagonalize the families of operators

$$\exp\left(i \sum_j c_j^{(k)} P_j^{(k)}\right) = V_k \exp\left(i \sum_j \tilde{c}_j^{(k)} \tilde{P}_j^{(k)}\right) V_k^\dagger\tag{15}$$

are given below in gate form. The remaining step in the derivation of the primitive gate sets for the $\mathcal{H}_{e/o}$, is the optimization of the exponentiated sum of diagonal terms $\exp(i \sum_j \tilde{c}_j^{(k)} \tilde{P}_j^{(k)})$. Here, optimization refers to the number of CNOT gates. Making use of the identity $Z_a \otimes Z_b = \text{CNOT}_{a,b} I_a \otimes Z_b \text{CNOT}_{a,b}$ and taking into account mutual cancellations between neighboring CNOTs, we arrive at the gate set for each of the four exponentiated families. As an example, the relevant gates for the exponentiation of the first family are displayed in Fig. 1, where the remaining sets are given in the [Appendix](#), Fig. 6. With the observation that the partitioning of the lattice Hamiltonian into mutually commuting sets of terms in nn -form (Eq. (12)) is easily generalized to higher dimensions, it can readily be seen that the derivation Eqs. (13)-(15), leading to the gate sets Figs. 1 and 6, holds in any dimension. We restrict ourselves to hypercubic lattice geometries which naturally arise in the context of staggered fermions [8].

3.2 Inclusion of baryons

Extending our theory from gauge group $U(3)$ to $SU(3)$ requires the extension of $|h\rangle = |m\rangle$ to $|h\rangle = |m, b\rangle$, as defined in Eq. (8). It is important to note that owing to the limit of infinite gauge coupling *and* continuous time, baryons remain static in our toy theory. Given an initial state $|\psi_0\rangle = \otimes_x |h\rangle_x$, the *time evolution* of bosonic and baryonic sites decouples

³We quote here the result of IBM Qiskit’s [24] `group_commuting` which uses a graph-coloring approach.

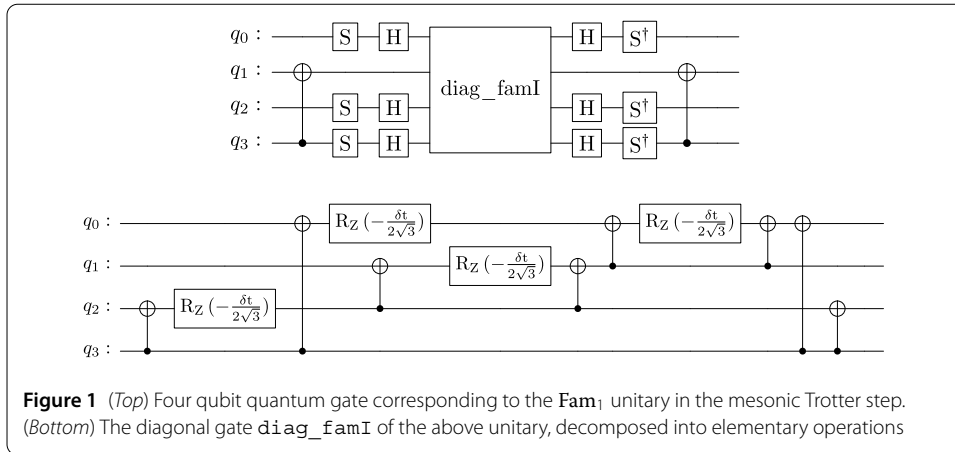


Figure 1 (Top) Four qubit quantum gate corresponding to the Fam_1 unitary in the mesonic Trotter step. (Bottom) The diagonal gate $diag_famI$ of the above unitary, decomposed into elementary operations

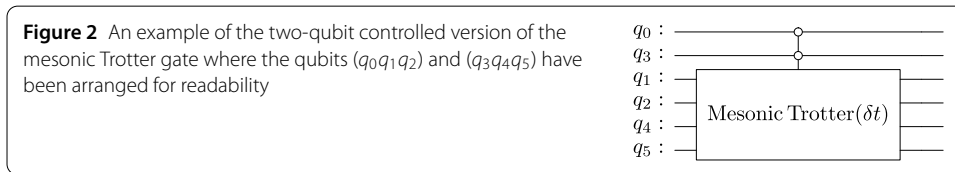


Figure 2 An example of the two-qubit controlled version of the mesonic Trotter gate where the qubits ($q_0q_1q_2$) and ($q_3q_4q_5$) have been arranged for readability

Table 1 Gate depth and CNOT count of a single mesonic Trotter gate acting on a pair of qubit registers, as displayed in Fig. 2

	Circuit depth	#CNOT
Fam_1	16	10
Fam_2	18	14
Fam_3	12	10
Fam_4	21	16
Total	67	50

as $[\mathcal{H}, \mathcal{N}] = 0$, with baryons evolving trivially, only leaving an imprint on the surrounding “pion bath” through a fixed excluded volume. From the practical side of quantum simulations this implies that the gate set identified so far is sufficient to capture the dynamics of the theory with gauge group $SU(3)$ in the zero-temperature limit.

At non-zero chemical potential or temperature, $\mu_B, T > 0$ we will need to extend our register to three qubits per site x to represent all six classical states $|\mathfrak{h}_i\rangle \in \{0, \pi, 2\pi, 3\pi, B^+, B^-\}$, with two states being redundant. As $\hat{\mathcal{H}}_{x_{e|o}}$ and $\hat{\mathcal{N}}_x$ act on this Hilbert space through a direct sum, we can use the three qubits in the register ($q_0q_1q_2$) and encode the hadronic sector (meson or baryon) of \mathfrak{h}_x in, say, q_0 , thus having it act as *control* bit. A *mesonic* Trotter step thus consists of the gates derived in the last section, Fig. 1 and Fig. 6, but in their controlled version (e.g. on “0”), with one control bit per site. The unitary $\exp(-i\delta t \hat{\mathcal{H}}_{x_{e|o}})$ acting on pairwise sets of qubits encoding $|\mathfrak{h}\rangle_x$ and $|\mathfrak{h}\rangle_y$ of nm -pairs $\langle x, y \rangle$, respectively, is hence represented by the symbolic circuit Fig. 2, where the gate depth and CNOT count are given in Table 1.

The baryon evolution is governed by a single operator in diagonal form (i.e. Z -term in the Hamiltonian) locally at a given site x through the term $\exp(-it \sum_x \hat{\omega}_x)$ and hence does not need to be Trotterized. We thus only have to take into account the local control bit denoted by q_0 (e.g. on “1”), which encodes the hadronic sector. Furthermore, in order to restrict the action of $\exp(-it\omega_x)$ to the $(B^+, B^-)^T$ part of $|\mathfrak{h}\rangle_x$ (encoded on q_2), we can add



a control by q_1 . This excludes the two redundant states of the $2^3 = 8$ possible classical states. This is depicted in Fig. 3, where one can see the only baryonic gate used in the time evolution of the full (SU(3)) theory.

3.3 Trotterized time evolution in $d = 1 + 1$

Approximating the time evolution by a first order product formula, the Trotterized time-evolution operator of our theory is as follows

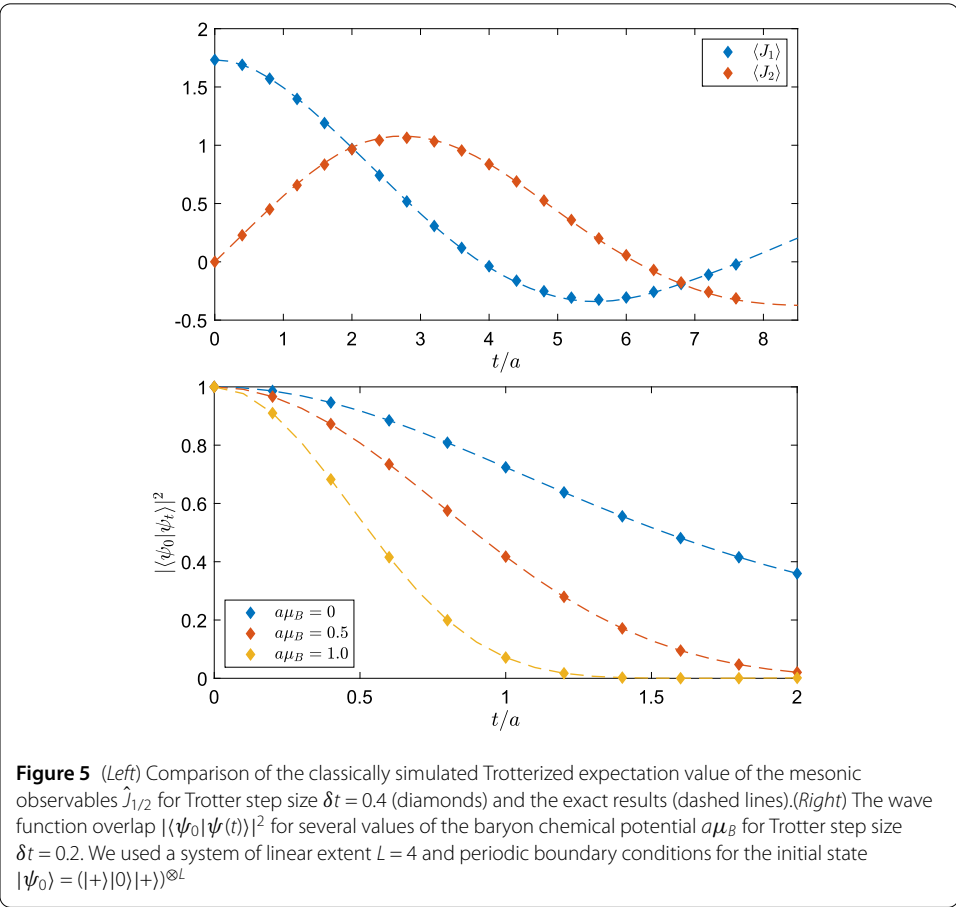
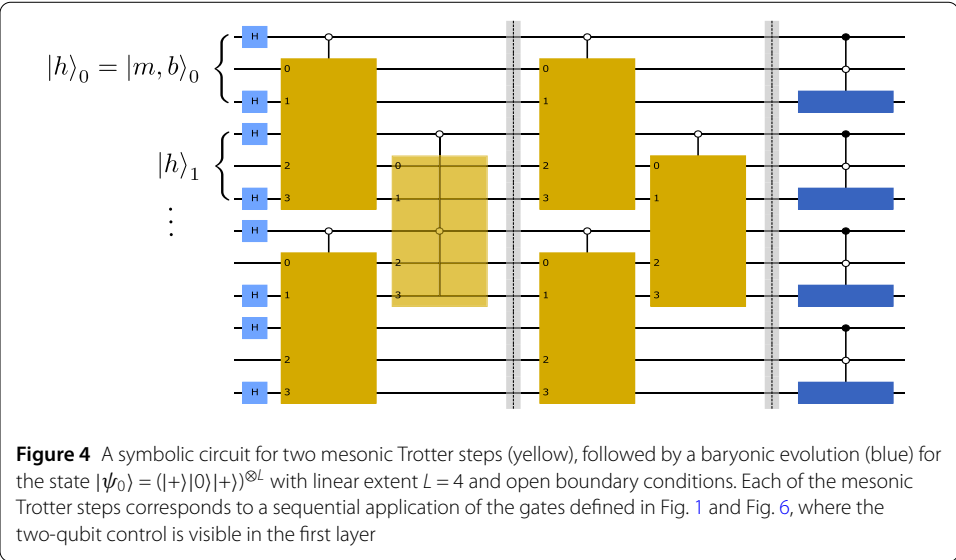
$$\hat{U}_{\text{Trott}}(t) = \left(e^{-i\delta t \sum_{x_e} \hat{H}_{x_e}} e^{-i\delta t \sum_{x_o} \hat{H}_{x_o}} \right)^N e^{+it\hat{N}a\mu_B}, \tag{16}$$

with a systematic error of order $\mathcal{O}(\delta t^2)$ for every Trotter step δt with $\delta t = t/N$. The symbolic circuit corresponding to the staggered layers of mesonic Trotter gates, followed by a baryonic evolution for a lattice of dimension $d = 1 + 1$ with linear extent $L = 4$ is depicted in Fig. 4. Here we have used open boundary conditions for illustrative purposes and chose the initial state $|\psi_0\rangle = \otimes_{i=0}^{L-1} (|+\rangle|0\rangle|+\rangle)$, where at each lattice site one has the following state in the hadron occupation basis $|\mathfrak{h}\rangle_x = \frac{1}{2}(1, 1, 0, 0, 1, 1)^T$, i.e. a superposition of states with non-zero mesonic and baryonic occupation numbers. The two layers of a single mesonic Trotter step result from the nm -decomposition of our lattice Hamiltonian (Eq. (12)). Increasing the dimensionality will add two layers per space dimension, corresponding to the increase in coordination number of our hypercubic lattice. The gate depth of a mesonic Trotter step hence grows linearly with increasing lattice dimension and is unaffected by the lattice volume N (cf. Table 1 for a single mesonic gate), whereas the number of qubits grows linearly, $n_q = 3N$. From the point of view of computational complexity this resource requirement can be compared to the qubit count of LGT in the local multiplet basis [2] at lowest truncation order $\Lambda_p = 1$ where we have $n_q \approx 2N \log_2(\Lambda_p + 1)$ for *pure* Yang-Mills theory, i.e. without matter.

To verify the correctness of our gate decomposition summarized in Fig. 4, we show in Fig. 5 a comparison of exact and Trotterized observables as a function of time t , with the initial state $|\psi_0\rangle$ on a lattice of $L = 4$ sites ($n_q = 12$ qubits) with periodic boundary conditions. The displayed results correspond to a noise-free classical simulation, assuming infinite shot statistics. Using these time-evolved states, we have computed the time-dependent expectation values of the mesonic observables $\hat{J}_{1/2}$ (left), defined in Eq. (9) as well as the overlap $|\langle \psi_0 | \psi(t) \rangle|^2$ (right) for several values of the baryon chemical potential $a\mu_B$. We observe good agreement with the exact results.

3.4 Scalability

It is instructive to compare our implementation proposal for quantum simulations of lattice QCD in the strong coupling limit to existing benchmarks at scale, s.a. the recently published study of lattice QED in $d = 1 + 1$ (i.e. the Schwinger model) with more than 100 qubits [26] on an IBM Heron processor. There, using a second order Trotter formula to implement the time evolution of the system, 14 Trotter steps were reached with total



CNOT-depth of 370. If we restrict ourselves to the case of a purely mesonic theory (thus using the gauge group $U(3)$ instead of $SU(3)$) and take our resource requirements given in Table 1 at face value, time evolution of our $d = 1 + 1$ dimensional theory with a layering as given in Fig. 4 will require a CNOT-depth of 88 per first order Trotter step, thus already

permitting 4-5 (depending on transpilation) Trotter steps on current hardware with comparable quantum volume as the mesonic theory requires 2 qubits per staggered lattice site. While this may seem less favorable, we emphasize that going to larger spatial dimension in our theory will only result in a linear increase in CNOT-depth without modification of the proposed gate set.

Turning to the full theory (gauge group $SU(3)$), the pertinent question is the hardware realization of multi-qubit-controlled gates, in view of the 2-qubit controlled version of the mesonic and baryonic gates, Figs. 2 and 3. Commonly, a decomposition is used [27] which for 2-qubit control would essentially triple the CNOT-depth per Trotter step. More promising would be the use of multi-qubit gates [28] on trapped-ion quantum computers which were demonstrated for the case of 3-qubit and 4-qubit gates with promising fidelity [29].

For actual quantum simulations our circuits displayed in Fig. 1 and Fig. 6 clearly will require the use of error mitigation techniques [30] s.a. zero noise extrapolation (ZEN) [31] and probabilistic error cancellation (PEC) [32] to counter the effect of noise in the form of decoherence and limited gate fidelities, in particular those of the 2-qubit entangling gates. To convert the a priori unknown noise channel into Pauli noise channels, Pauli-twirling can be applied [33]. An additional hardware limitation, for a given spatial dimension, is the required qubit connectivity introduced by the dimensionality of the Hilbert space requiring 3 qubits per site to be coupled to the qubits of neighboring sites.

4 Conclusion and outlook

In summary, we have mapped the Hamiltonian for strong-coupling lattice QCD with one flavor of staggered quarks to qubit degrees of freedom by writing down the complete gate set to simulate its dynamics on a quantum computer. This formulation serves as a preparatory step to actual studies of the model on quantum hardware, where it is evident that this will not only allow one to study the dynamics of the model but also its thermal and finite-density properties, using e.g. thermal pure quantum states [34, 35] or the variational methods described in [36] and [37]. Strong-coupling lattice QCD is studied on classical computers via the Worm algorithm, introduced in [38] and first applied to $SU(3)$ in [14], which is based on the high-temperature expansion of the partition function. It is very efficient at high and intermediate temperatures, but not at low temperatures. Here, quantum simulations might be expected to outperform classical algorithms relying on importance sampling.

Repeating this exercise for $N_f > 1$ is another avenue to pursue. Considering the state multiplicity diagram given in [18] for $N_f = 2$, one sees that the purely bosonic sector of the theory ($|B| = 0$) will require the use of six qubits per lattice site and in the case a baryon is present ($|B| = 1$) will require five qubits. As the mesonic ladder operators \hat{J}^\pm remain block-diagonal and commute with the number operator, the mesonic trotter steps will not change the baryon number. While the gate set for the $N_f = 1$ Hamiltonian is well suited for superconducting quantum computers as the scalability analysis has shown, the quantum gate sets for $N_f = 2$ may require a different strategy: It may be advantageous to map the system to an effective theory or to make use of a qudit as a multi-level computational unit [39], suggesting that a quantum hardware based on trapped ions may be preferable. It should also be mentioned that our approach has limitations: the dual formulation for

staggered fermions requires an unimproved fermion action, and as it does not involve a fermion determinant, we cannot implement rooting.

The most physically relevant extension of the current work would be the inclusion of gauge corrections to the Hamiltonian formulation. This would allow one to make contact to other effective theories in the strong-coupling limit [11], and in the longer term, approach the continuum limit $a \rightarrow 0$. The dimension of the $N_f = 1$ Hilbert space at finite β becomes 16-dimensional. Higher order corrections will mainly contribute to the matrix elements of the ladder operators, resulting in a larger number of mutually commuting families. While the leading order gauge correction may still be suited for superconducting qubits, higher orders may result in a CNOT depth, for which other computational devices are beneficial. It should be stressed that both extensions of our Hamiltonian formulation still result in finite-dimensional Hilbert spaces, given N_f and a fixed order in the strong coupling expansion, with no further truncations required.

Appendix: Full gate sets

The coefficients c_i of the Pauli string decomposition $\mathcal{H}_{x_{e/o}} = \sum_i c_i P_i$ are given by $c_i = \frac{1}{2^4} \text{tr}(P_i \mathcal{H}_{e/o})$. After partitioning the entire set of Pauli strings into families of mutually commuting operators, we obtain the following result for the coefficients for the various families

$$\begin{aligned}
 c_i^{(1)} &= -\frac{v_L v_T}{8} = -\frac{1}{4\sqrt{3}}, \\
 c_i^{(2)} &\in \{-\phi_2, \phi_2, -\phi_2, \phi_2\}, \quad \phi_2 = \frac{v_T^2}{16} = \frac{1}{12}, \\
 c_i^{(3)} &\in \{-\phi_3, \phi_3, -\phi_3, \phi_3\}, \quad \phi_3 = \frac{v_L v_T}{8} = \frac{1}{4\sqrt{3}}, \\
 c_i^{(4)} &\in \{\phi_4^{(1)}, \phi_4^{(1)}, \phi_4^{(2)}, \phi_4^{(2)}, \phi_4^{(1)}, \phi_4^{(1)}\}, \\
 \phi_4^{(1)} &= -\frac{v_T^2}{16} = -\frac{1}{12}, \quad \phi_4^{(2)} = -\frac{v_L^2}{4} = -\frac{1}{4}.
 \end{aligned} \tag{17}$$

The diagonalization of the various families may change the sign of the coefficients, yielding

$$\begin{aligned}
 \tilde{c}_i^{(1)}, \tilde{c}_i^{(3)} &= -\frac{1}{4\sqrt{3}}, \\
 \tilde{c}_i^{(2)} &\in \{\phi_2, -\phi_2, -\phi_2, \phi_2\}, \\
 \tilde{c}_i^{(4)} &\in \{\phi_4^{(1)}, -\phi_4^{(1)}, \phi_4^{(2)}, -\phi_4^{(2)}, \phi_4^{(1)}, -\phi_4^{(1)}\}.
 \end{aligned} \tag{18}$$

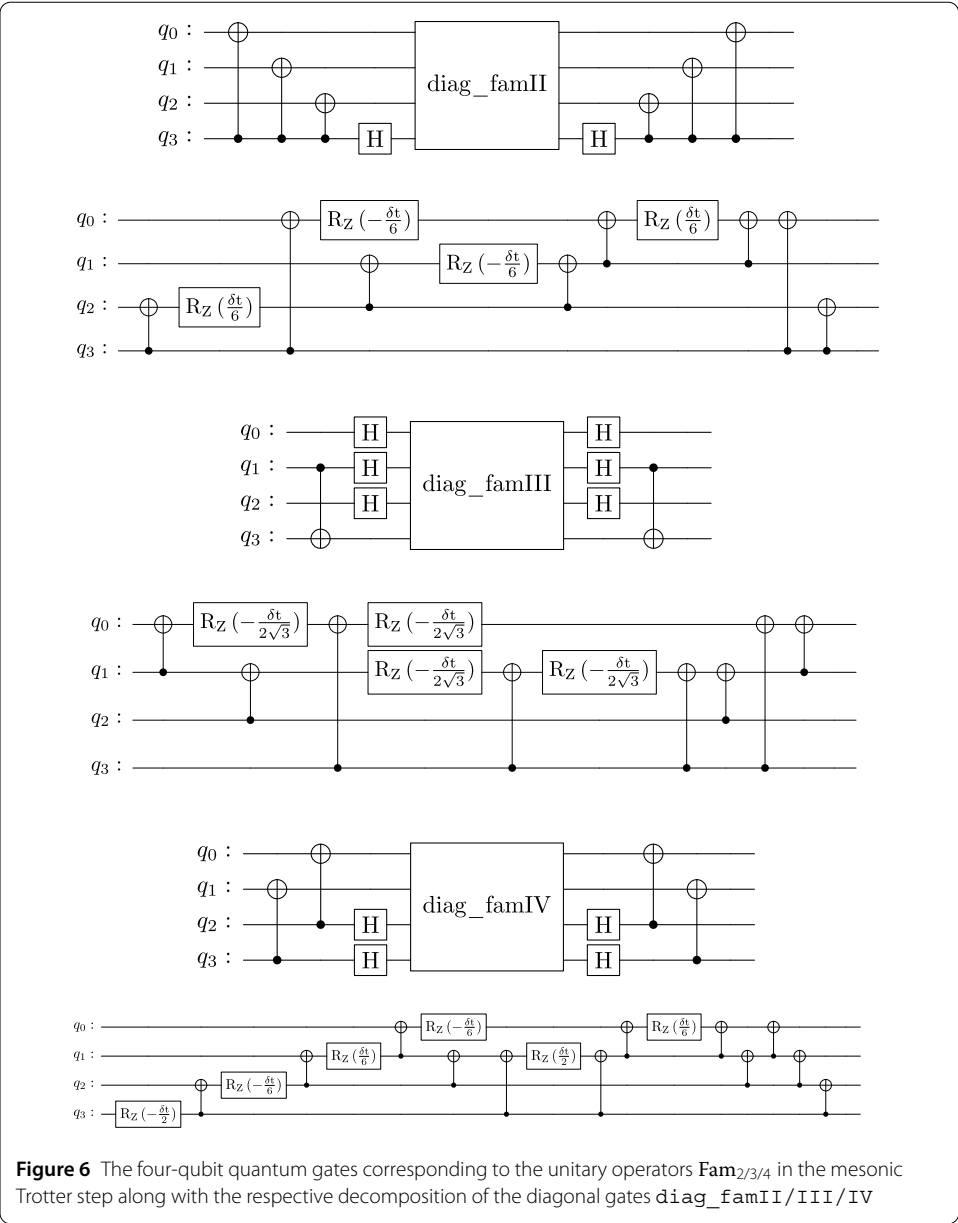


Figure 6 The four-qubit quantum gates corresponding to the unitary operators $Fam_{2/3/4}$ in the mesonic Trotter step along with the respective decomposition of the diagonal gates **diag_famII/III/IV**

Abbreviations
 QCD, Quantum Chromodynamics; QED, Quantum Electrodynamics.

Author contributions
 All authors contributed equally in the conception phase, C.W., M.F. and W.U. carried out the computations and simulations. All authors jointly drafted and reviewed the manuscript and approved the submission.

Funding
 Open Access funding enabled and organized by Projekt DEAL. The work is supported by the Deutsche Forschungsgemeinschaft (DFG, German Research Foundation) through the grant CRC-TR 211 “Strong-interaction matter under extreme conditions” – project number 315477589 – TRR 211 and by the State of Hesse within the Research Cluster ELEMENTS (Project ID 500/10.006).

Data availability
 Simulation data are available from the corresponding author upon reasonable request.

Declarations

Ethics approval and consent to participate

Not applicable.

Consent for publication

Not applicable.

Competing interests

The authors declare no competing interests.

Author details

¹Institut für Theoretische Physik, Goethe-Universität, Frankfurt am Main, Germany. ²Fakultät für Physik, Bielefeld University, Bielefeld, Germany.

Received: 19 October 2023 Accepted: 19 March 2024 Published online: 25 March 2024

References

1. Lamm H, Lawrence S, Yamauchi Y. General methods for digital quantum simulation of gauge theories. *Phys Rev D*. 2019;100(3):034518. <https://doi.org/10.1103/physrevd.100.034518>.
2. Klco N, Stryker JR, Savage MJ. $SU(2)$ non-Abelian gauge field theory in one dimension on digital quantum computers. *Phys Rev D*. 2020;101:074512. <https://doi.org/10.1103/PhysRevD.101.074512>. arXiv:1908.06935.
3. Ciavarella A, Klco N, Savage MJ. Trailhead for quantum simulation of $SU(3)$ Yang-Mills lattice gauge theory in the local multiplet basis. *Phys Rev D*. 2021;103(9):094501. <https://doi.org/10.1103/physrevd.103.094501>.
4. Davoudi Z, Raychowdhury I, Shaw A. Search for efficient formulations for Hamiltonian simulation of non-Abelian lattice gauge theories. *Phys Rev D*. 2021;104:074505. <https://doi.org/10.1103/PhysRevD.104.074505>. arXiv:2009.11802.
5. Halimeh JC, Homeier L, Bohrdt A, Grusdt F. Spin exchange-enabled quantum simulator for large-scale non-Abelian gauge theories. 2023. <https://doi.org/10.48550/ARXIV.2305.06373>. arXiv:2305.06373.
6. Kan A, Nam Y. Lattice quantum chromodynamics and electrodynamics on a universal quantum computer. 2021. <https://doi.org/10.48550/ARXIV.2107.12769>. arXiv:2107.12769.
7. Preskill J. Quantum computing in the NISQ era and beyond. *Quantum*. 2018;2:79. <https://doi.org/10.22331/q-2018-08-06-79>.
8. Kogut J, Susskind L. Hamiltonian formulation of Wilson's lattice gauge theories. *Phys Rev D*. 1975;11(2):395–408. <https://doi.org/10.1103/physrevd.11.395>.
9. Byrnes T, Yamamoto Y. Simulating lattice gauge theories on a quantum computer. *Phys Rev A*. 2006;73(2):022328. <https://doi.org/10.1103/physreva.73.022328>.
10. Zohar E, Burrello M. Formulation of lattice gauge theories for quantum simulations. *Phys Rev D*. 2015;91(5):054506. <https://doi.org/10.1103/physrevd.91.054506>.
11. Ciavarella AN. Quantum simulation of lattice QCD with improved Hamiltonians. 2023. <https://doi.org/10.48550/ARXIV.2307.05593>. arXiv:2307.05593.
12. Rossi P, Wolff U. Lattice QCD with fermions at strong coupling: a dimer system. *Nucl Phys B*. 1984;248(1):105–22. [https://doi.org/10.1016/0550-3213\(84\)90589-3](https://doi.org/10.1016/0550-3213(84)90589-3).
13. Karsch F, Mütter K-H. Strong coupling QCD at finite baryon-number density. *Nucl Phys B*. 1989;313(3):541–59. [https://doi.org/10.1016/0550-3213\(89\)90396-9](https://doi.org/10.1016/0550-3213(89)90396-9).
14. de Forcrand P, Fromm M. Nuclear physics from lattice QCD at strong coupling. *Phys Rev Lett*. 2010;104(11):112005. <https://doi.org/10.1103/physrevlett.104.112005>.
15. de Forcrand P, Langelage J, Philipsen O, Unger W. Lattice QCD phase diagram in and away from the strong coupling limit. *Phys Rev Lett*. 2014;113(15):152002. <https://doi.org/10.1103/physrevlett.113.152002>.
16. Klegrew M, Unger W. Strong coupling lattice QCD in the continuous time limit. *Phys Rev D*. 2020;102(3):034505. <https://doi.org/10.1103/physrevd.102.034505>.
17. Pattanaik P, Unger W. Hamiltonian lattice QCD from strong coupling expansion. 2021. <https://doi.org/10.48550/ARXIV.2112.11875>. arXiv:2112.11875.
18. Pattanaik P, Unger W. Towards quantum Monte Carlo simulations at non-zero baryon and isospin density in the strong coupling regime. 2022. <https://doi.org/10.48550/ARXIV.2212.11328>. arXiv:2212.11328.
19. Bollweg D, Klegrew M, Unger W. Thermodynamics at strong coupling on anisotropic lattices. 2018. <https://doi.org/10.48550/ARXIV.1811.03584>. arXiv:1811.03584.
20. de Forcrand P, Unger W, Vairinhos H. Strong-coupling lattice QCD on anisotropic lattices. *Phys Rev D*. 2018;97:034512. <https://doi.org/10.1103/PhysRevD.97.034512>.
21. Klegrew M. Strong coupling lattice QCD in the continuous time limit. 2020. <https://doi.org/10.4119/UNIBI/2944679>.
22. Gagliardi G, Unger W. New dual representation for staggered lattice QCD. *Phys Rev D*. 2020;101(3):034509. <https://doi.org/10.1103/PhysRevD.101.034509>. arXiv:1911.08389.
23. Murairi EM, Cervia MJ, Kumar H, Bedaque PF, Alexandru A. How many quantum gates do gauge theories require? 2022. arXiv:2208.11789.
24. Qiskit contributors. Qiskit: an open-source framework for quantum computing. 2023. <https://doi.org/10.5281/zenodo.2573505>.
25. van den Berg E, Temme K. Circuit optimization of Hamiltonian simulation by simultaneous diagonalization of Pauli clusters. *Quantum*. 2020;4:322. <https://doi.org/10.22331/q-2020-09-12-322>.
26. Farrell RC, Illa M, Ciavarella AN, Savage MJ. Quantum simulations of hadron dynamics in the schwinger model using 112 qubits. 2024. <https://doi.org/10.48550/ARXIV.2401.08044>. arXiv:2401.08044.
27. Barenco A, Bennett CH, Cleve R, DiVincenzo DP, Margolus N, Shor P, Sleator T, Smolin JA, Weinfurter H. Elementary gates for quantum computation. *Phys Rev A*. 1995;52(5):3457–67. <https://doi.org/10.1103/physreva.52.3457>.
28. Katz O, Cetina M, Monroe C. n -body interactions between trapped ion qubits via spin-dependent squeezing. *Phys Rev Lett*. 2022;129(6):063603. <https://doi.org/10.1103/physrevlett.129.063603>. arXiv:2202.04230.

29. Katz O, Feng L, Risinger A, Monroe C, Cetina M. Demonstration of three- and four-body interactions between trapped-ion spins. *Nat Phys*. 2023;19(10):1452–8. <https://doi.org/10.1038/s41567-023-02102-7>. arXiv:2209.05691.
30. Temme. With fault tolerance the ultimate goal, error mitigation is the path that gets quantum computing to usefulness. Technical report. <https://research.ibm.com/blog/gammabar-for-quantum-advantage>.
31. Li Y, Benjamin SC. Efficient variational quantum simulator incorporating active error minimisation. *Phys Rev X*. 2017;7(2):021050. <https://doi.org/10.1103/physrevx.7.021050>. arXiv:1611.09301.
32. Gupta RS, van den Berg E, Takita M, Riste D, Temme K, Kandala A. Probabilistic error cancellation for dynamic quantum circuits. 2023. <https://doi.org/10.48550/ARXIV.2310.07825>. arXiv:2310.07825.
33. Wallman JJ, Emerson J. Noise tailoring for scalable quantum computation via randomized compiling. *Phys Rev A*. 2016;94(5):052325. <https://doi.org/10.1103/physreva.94.052325>. arXiv:1512.01098.
34. Powers C, Oftelie LB, Camps D, de Jong WA. Exploring finite temperature properties of materials with quantum computers. 2021. arXiv:2109.01619.
35. Davoudi Z, Mueller N, Powers C. Toward quantum computing phase diagrams of gauge theories with thermal pure quantum states. 2022. arXiv:2208.13112.
36. Cerezo M, Arrasmith A, Babbush R, Benjamin SC, Endo S, Fujii K, McClean JR, Mitarai K, Yuan X, Cincio L, Coles PJ. Variational quantum algorithms. *Nat Rev Phys*. 2021;3(9):625–44. <https://doi.org/10.1038/s42254-021-00348-9>. arXiv:2012.09265.
37. Verdon G, Marks J, Nanda S, Leichenauer S, Hidary J. Quantum Hamiltonian-based models and the variational quantum thermalizer algorithm. 2019. arXiv:1910.02071.
38. Prokof'ev N, Svistunov B. Worm algorithms for classical statistical models. *Phys Rev Lett*. 2001;87:160601. <https://doi.org/10.1103/PhysRevLett.87.160601>.
39. Wang Y, Hu Z, Sanders BC, Kais S. Qudits and high-dimensional quantum computing. *Front Phys*. 2020;8:479. <https://doi.org/10.3389/fphy.2020.589504>. arXiv:2008.00959.

Publisher's Note

Springer Nature remains neutral with regard to jurisdictional claims in published maps and institutional affiliations.

Submit your manuscript to a SpringerOpen[®] journal and benefit from:

- Convenient online submission
- Rigorous peer review
- Open access: articles freely available online
- High visibility within the field
- Retaining the copyright to your article

Submit your next manuscript at ► [springeropen.com](https://www.springeropen.com)
